Supersonic flow over three dimensional cavities

R. Das
rishi.aero@gmail.com
J. Kurian
kurian@iitm.ac.in
Indian Institute of Technology, Madras
Chennai, India

ABSTRACT

This work presents a study of acoustic oscillations generated and the wave structure associated with supersonic flow past wall mounted 3D open cavities of varying length-to-width (L/W) ratio. Experiments were conducted to investigate the acoustic signature generated by the cavities at freestream Mach number of 1·7. The effect of L/W ratio of the cavity on the dominant modes of the acoustic signature registered on different walls of the cavities is investigated for an L/W range of 0·83-4. Shift in the dominant acoustic mode is observed as L/W ratio changes from 3 to 4. Statistical analysis of pressure data showed existence of acoustic waves and spreading of acoustic energy over different modes with change in cavity width. Time averaged schlieren visualisation indicated variation of shock and shear layer structure in the mainstream for the different cavities. Acoustic waves generated by the presence of the cavity and the dynamic behaviour of the shear layer were observed during instantaneous shadowgraph visualisation. Numerical simulation was done to make a prior assessment of the flow structure and the results are in good agreement with those from experiments. Ratio of mass exchange between cavity and mainflow and the cavity volume was observed to have profound effect on the magnitude of pressure oscillations generated by the cavities.

Paper No. 3811. Manuscript received 10 January 2012, revised version received 2 May 2012, accepted 10 May 2012.

https://doi.org/10.1017/S0001924000007934 Published online by Cambridge University Press

NOMENCLATURE

A	facet area
D	depth of cavity
f	frequency in Hz
i	facet number
k_c	ratio of speed of convection of shed vortices to freestream speed
L	length of cavity
M_∞	freestream Mach number
m	mode number
m_c	mass flow rate between cavity and freestream
n	total number of facets
P_{rms}	root mean square pressure
SPL	sound pressure level in dB
St	Strouhal number
V_c	volume of cavity
V_∞	freestream velocity
v	local velocity of flow
W	width of cavity
α	shock wave angle
β	shear layer deflection angle
ε	m_c / V_c ratio
ξ	time lag in phase relation
η	non-dimensionalised cross correlation coefficient
ρ	fluid density

1.0 INTRODUCTION

Physical mechanism associated with the flow past cavities has received considerable attention in the past decades mostly in connection with the pressure loadings on aircrafts and also with the potential for enhancement of fuel air mixing and flame holding in supersonic combustors. External cut outs like wheel and bomb bays, similar to cavities exist on the body of aerospace vehicles. They cause the flow over the body to separate and produce complex wave systems, reattachment, vortical flow structures and other complex flow phenomena. This leads to unwanted pressure loadings on the vehicle surface causing structural damage and aerodynamic instabilities. Characteristics of such flow are determined by the flow conditions and by the cavity geometry. Studies have been conducted to understand and interpret this complex flow mechanism and in particular to find ways to reduce unwanted loads on vehicle surfaces. Cavities have also been projected as mixing and flame holding devices for supersonic combustion engines as mixing between compressible streams is characterised by slow overall kinetic rates and short combustor residence time. The unsteadiness in the flow generated by cavities and the consequent emission of acoustic oscillations is considered as a potential tool to enhance fuel-air mixing process.

Extensive studies on wall mounted cavity flow by numerous researchers have been done previously. Existence of an oscillatory shear layer and coupling of the acoustic oscillations with a feed back mechanism has been well established by early researchers[1,2]. Dependency of the modal frequencies of oscillations on cavity geometry is underlined in the semi-empirical formula proposed by Rossiter which was later modified by Heller *et al*[3]. Periodic inflow and outflow of

https://doi.org/10.1017/S0001924000007934 Published online by Cambridge University Press

fluid in the cavity due to the fluctuating motion of the shear layer has been considered as the driving mechanism for cavity oscillations[4].

Unsteadiness in the flow field produced by emission of acoustic oscillations from wall mounted cavities has been proposed as an effective tool to enhance fuel air mixing. Transverse acoustic oscillations generated by cavities have been found to affect mixing processes in supersonic streams[5,6]. Rockwell and Naudauscher[7] have classified the oscillation mechanism in three distinct categories. Of importance to the present work is their classification of fluid dynamic and fluid resonant mechanisms of cavity oscillations which exist under certain geometrical conditions. Flow field in the vicinity of the cavity has been found to be dominated by the waves generated in the mainstream and inside the cavity. Transient nature of flow at the trailing edge causes emission of compression waves which propagate from the trailing edge[8]. As the shear layer dives into the cavity at the trailing edge, thereby exposing the edge to the supersonic flow, a bow shock is formed near the trailing edge[9].

Investigations on cavity flows have been mostly restricted to cavities spanning the entire width of the test section, with a few investigators studying the flow over cavities with width lesser than that of the flow channel. The wall mounted cavities with width less than that of the flow path are referred to as partially spanning cavities in this paper. For flow over such cavities, pressure oscillations and spanwise vortical structures inside the cavity have been found to change with cavity width for low subsonic velocities[10,11]. Flow over partially spanning cavities was found to oscillate primarily in the shear layer mode according to the results of numerical simulation by Sheih and Morris[12]. Existence of multiple peaks of pressure oscillations inside the cavity was observed for supersonic free stream flow at $M_\infty = 1{\cdot}2$[13]. Large scale structures have been observed over a partially spanning cavity during shadowgraph visualisation for Mach 2 flow over the cavity[14]. Suppression of vibrations by the sidewalls and existence of multiple peaks for cavities has been reported by Choi *et al*[15]. Woo *et al* numerically investigated the flow field around cavities at freestream $M_\infty = 1{\cdot}5$ and concluded that the mode of the dominant frequency changes as the width of the cavity was changed[16].

The present work is carried out to gain an insight into the flow structure in and around partially spanning wall mounted open cavities in a rectangular duct through which supersonic flow of Mach number $M_\infty = 1{\cdot}7$ is maintained. Literature on partially spanning cavities under supersonic flow conditions is scant and the present work aims to fill the gap to some extent. Open cavities with lower L/D ratio of 2 are used in the present study. It has been observed that transverse acoustic oscillations generated by lower L/D ratio cavities provide enhanced mixing in supersonic flows by positively influencing the shear layer growth[5]. Residence time of flow inside the cavity has been observed to be a direct function of the mass exchange rate in and out of the cavity. Cavity residence time has been observed to be larger for cavities with lower L/D ratio[17]. Cavities find applications as flame holding devices too in scramjet combustors. At higher L/D ratios drag induced by cavities is larger due to increase in pressure at the cavity trailing edge and subsequent drop in time mean pressure at the leading edge wall of the cavity[18]. Thus for ideal scramjet combustors where lower drag, higher flow residence time and better mixing are desirable, cavities with lower L/D ratios are suggested to be employed. The present work is further targeted to study the effect of cavity width on the acoustic field generated in its vicinity. Making use of the experimental results, an attempt is made to explain the physical aspects of the flow. A comparative study of such cavities with different widths has been carried out through statistical analysis of the data obtained.

https://doi.org/10.1017/S0001924000007934 Published online by Cambridge University Press

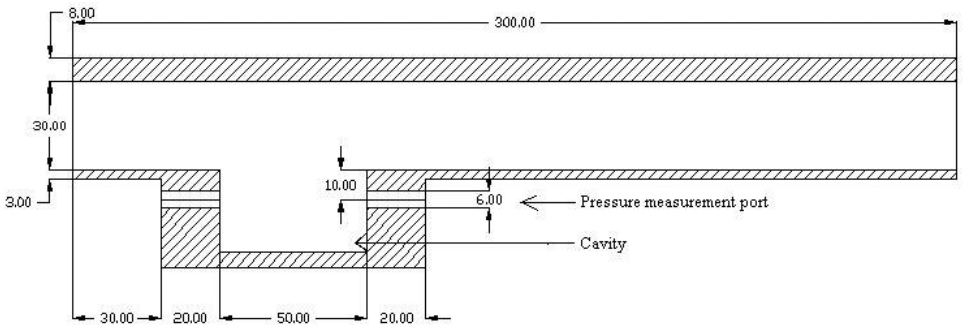


Figure 1. Schematic of test section.

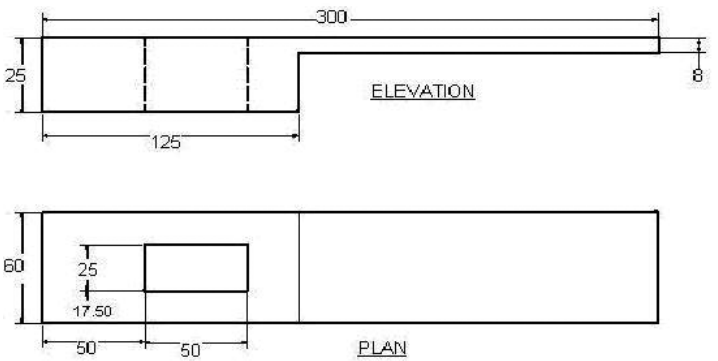


Figure 2. Bottom plate of the test section.

2.0 EXPERIMENTAL DETAILS

Schematic of the test section along the axial plane is shown in Fig. 1. The Mach 1·7 flow is maintained in the test section of cross section 60 × 30mm^2 at a flow Reynolds number of 1·1805e06 based on the cavity length and the numerically calculated freestream velocity. Cavities of length 50mm and depth 25mm were used for the study. The width of the cavities were kept at 60mm, 25mm, 16·7mm and 12·5mm in different sets of experiments thereby giving L/W ratios of 0·83(5/6), 2, 3 and 4 for the test cases. The L/D ratio of the cavity was kept constant at 2 for all the cases. A 2D view of the floor of the test section showing the open top of the partially spanning cavity of $L/W = 2$ and the other details are shown in Fig. 2. A 3D isometric view of the test section is shown in Fig. 3.

Unsteady pressure measurements were done using piezoelectric type transducers of PCB make (PCB Piezotronics, model 112A22). Two transducers were used to make measurements at two ports of the cavity simultaneously. An NI-6024E A/D converter card was used to acquire the signals from the transducers. The maximum sampling frequency of the card was 200kS/sec and a sampling rate of 100kS/sec was available for each of the transducers. Signals were acquired for 0·5 sec thereby giving 50,000 samples for each run. The locations of the measurement ports on the partially spanning cavity walls are shown in Fig. 4 in an exploded view of the cavity. The sidewall ports are numbered from 1 to 6. The ports 1 and 4 are closer to the trailing edge. Measurements were done at the leading and trailing edge pressure ports for the cavity spanning the entire width of the

https://doi.org/10.1017/S0001924000007934 Published online by Cambridge University Press

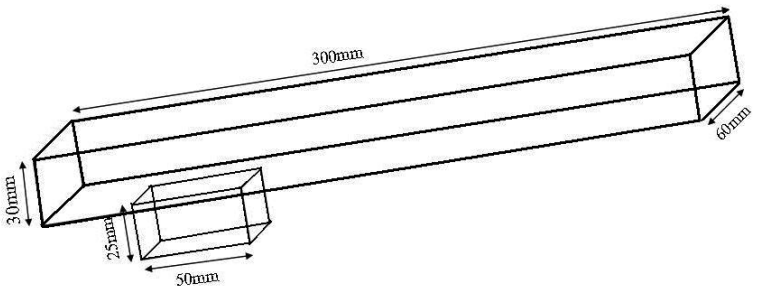


Figure 3. Schematic diagram of three-dimensional cavity configuration.

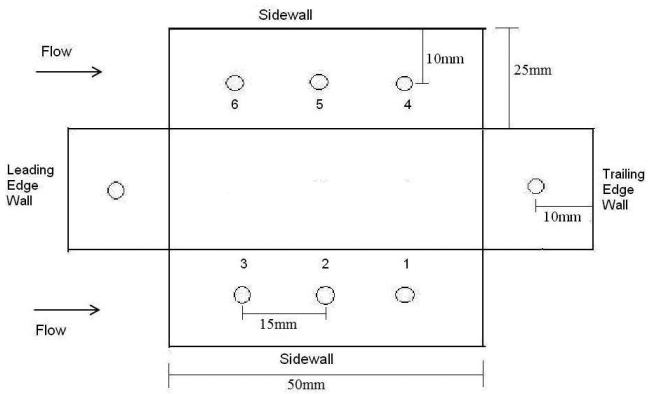


Figure 4. Pressure ports on cavity walls (opened up in horizontal and lateral plane along cavity floor).

test section (baseline model). Measurements along sidewall ports for the baseline model was not considered for the current study as exchange of fluid between the cavity and the mainstream along the cavity sidewalls will be constrained in this case. Generation of pressure oscillations depends on the inflow and outflow of fluid mass at the trailing edge for such cavities[19]. The acquired signals were processed through a Matlab program where FFT algorithm was employed to identify the dominant frequencies and their amplitudes. Each data record was windowed into 48 segments of 1,024 samples each with a transform length of 2,048 samples. A Hamming window with 50% overlap is used for estimation of the spectra giving a frequency resolution of 48·82Hz. Multiple runs were conducted under identical experimental conditions, under which variation in the frequencies of the dominant modes were observed to be within 10Hz in the 0 to 50KHz range. Experimental uncertainty in measuring amplitudes of the dominant modes was found to be within ±3%. This is obtained by ensemble average of about 24 data sets with 2,048 points each.

Time averaged colour schlieren visualisation is performed in the vicinity of the cavity. A 50W quartz tungsten halogen lamp is used as a constant point light source and an Olympus digital camera is used to obtain the time averaged images. Instantaneous shadowgraph imaging is done to study the transient nature of the flow in the vicinity of the cavity. A strobe light producing spark of 18ns duration at a maximum flashing rate of 20kHz was used in the experiments. A CMOS camera (Redlake, model N-4) capable of capturing 4,000 frames/sec at maximum resolution is used to capture the images at a framing rate of 1,500 frames per second and an exposure time of 74μs.

https://doi.org/10.1017/S0001924000007934 Published online by Cambridge University Press

3.0 RESULTS AND DISCUSSION

3. 1 Unsteady pressure measurements

The fluctuating pressure data obtained at various ports on the cavity walls were analysed by Fourier transformation to determine the Strouhal number (*St*) of the modes of oscillation present in the flow. The obtained *St* is compared with it's theoretically obtained value given by modified Rossiter's formula[3]. The modified Rossiter's formula for prediction of mode frequencies is given as follows:

$$St = \frac{fL}{V_\infty} = \frac{m - \xi}{\dfrac{\mathrm{M}_\infty}{\sqrt{1 + \dfrac{\gamma - 1}{2}\mathrm{M}_\infty^2}} + \dfrac{1}{k_c}} \qquad \ldots (1)$$

The above equation was proposed considering negligible error involved in assuming that the cavity temperature and the freestream stagnation temperature are equal at lower Mach numbers. In the present study, d.epending on the flow conditions and the geometrical aspects of the cavities, the values of ξ and k_c are taken as 0·25 and 0·57 respectively. The freestream velocity V_∞ is 490ms^{-1} as was measured earlier using Laser Doppler Velocimeter during the course of this study. The length of the cavity was kept constant for all the models and the width varied in the case of different models. *St* for different modes were calculated based on both cavity length and width. The values of *St* thus obtained both experimentally and theoretically are plotted and shown in Fig. 5 for the partially spanning models.

Experimentally obtained values of *St* of each of the mode based on cavity length shows good agreement with the theoretical values for the first five modes of oscillation that is observed to exist within the cavity. The values of *St* obtained based on the cavity width is observed to be much lower than the theoretically predicted values. The good agreement of *St* obtained from experimental data and that calculated based on cavity length show the dependency of discrete oscillation frequency on the cavity length. Existence of these discrete modes for all the models irrespective of the width of the cavity signifies that cavity width does not govern the existence of different oscillation modes. However, this does not necessarily imply that the nature of the various modes of oscillation will be independent of the cavity width.

To further investigate the nature of oscillations generated by cavities of different widths, spectra of pressure signal obtained at the trailing edge port of each of the cavities are plotted against the Strouhal number, *St* and shown in Fig. 6. Fluctuating pressure has been non-dimensionalised by the freestream static pressure of the incoming flow. Occurrence of discrete magnitude peaks along with broadband fluctuations is observed in all the spectra. Existence of peaks and their periodicity emphasise a periodic wave structure in all the cavities. Generation of these waves is due to the dynamic nature of the shear layer and its interaction with the trailing edge. From Fig. 6 it is evident that as the cavity became narrower, the dominant pressure oscillation moved to a mode at a different frequency. This change of frequency of the dominant mode is dependent on the width of the cavity.

Similar results are reported in earlier numerical investigations[16]. Such jump in frequency can be explained on the basis of fluid resonant effect due to reflection of acoustic waves from the cavity walls[20]. A sharp change in amplitude of the dominant mode is also observed as the cavity *L*/*W* ratio changes from 2 to 3. Frequency of the dominant wave was observed to be same for the *L*/*W*

https://doi.org/10.1017/S0001924000007934 Published online by Cambridge University Press

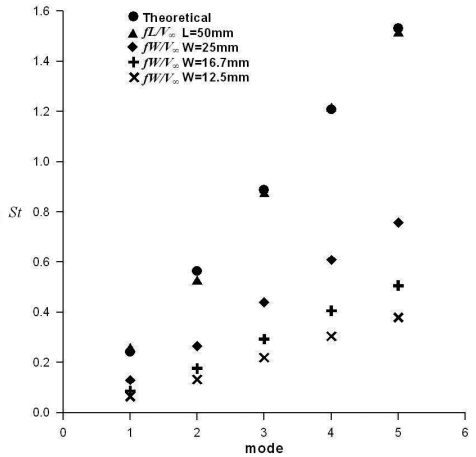


Figure 5. Comparison of experimental and modified Rossiter's mode *St*.

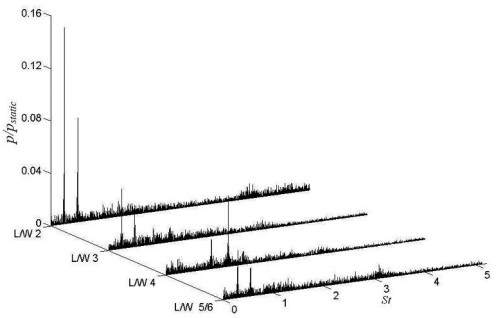


Figure 6. Spectra of pressure oscillations (trailing edge) of cavities.

Table 1
Frequency and SPL of oscillations of discrete modes observed at the trailing edge

Mode	Frequency	*St*	SPL (dB)			
	(Hz)	(fL/V_∞)	L/W 2	$L/W = 3$	$L/W = 4$	L/W = 5/6
1	2,542	0·259	177·6	169·2	154·9	169·5
2	5,181	0·529	172·1	164·1	–	–
3	8,602	0·878	–	155·9	161·0	–
4	11,930	1·217	–	154·9	168·6	–
5	14,860	1·516	–	151·6	154·1	–

= 2 and $L/W = 3$ cavities corresponding to *St* 0·259 based on the cavity length. Similarly for the baseline cavity with L/W = 5/6, the fundamental mode of oscillation is found to be dominant as showed in Fig. 6. Apart from the narrowest cavity, the discrete high amplitude peaks for the wider cavities were observed to be restricted to the fundamental and first harmonic modes corresponding to *St* 0·259 and 0·529 respectively.

A comparative study of the values of the amplitudes and frequency of the discrete peaks of oscillations at the trailing edge for all the cavities is shown in Table 1. It is observed that the sound pressure level (SPL) = 20log (P_{rms}/20μPa) of pressure oscillation of the dominant mode for the $L/W = 2$ cavity is 177·6dB at *St* 0·259 and is the highest among the cavities. In comparison with the cavity of L/W ratio 2, the magnitude of the dominant mode for the baseline cavity was observed to be much lower at 169·5dB at *St* 0·259. The second and the third modes of oscillations for the baseline cavity were observed to be at *St* 0·548 and 0·907 with an SPL of 164·6dB and 158·3dB respectively.

The higher modes for the baseline cavity that spans the entire width of the test section corresponds to Strouhal number that are higher than the predicted value by modified Rossiter's formula. The *St* values obtained for the various modes of oscillations of the partially spanning cavities are observed to be in better agreement with those predicted by modified Rossiter's formula.

https://doi.org/10.1017/S0001924000007934 Published online by Cambridge University Press

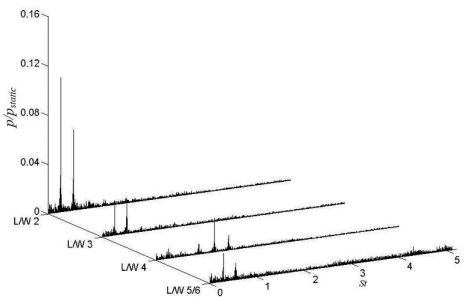


Figure 7. Amplitude spectra of pressure oscillations (leading edge) of cavities.

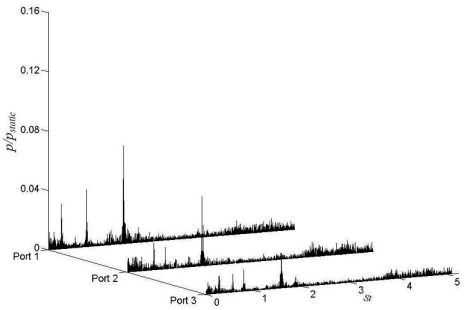


Figure 8. Amplitude spectra of pressure oscillation (sidewall ports of $L/W = 2$ model).

Amplitude spectrum for the leading edge pressure port is shown in Fig. 7. It is observed that the dominant modes are same as the trailing edge with only a decrease in amplitude of all the modes. The frequency of different modes of oscillations at leading and trailing edge is observed to be identical for each of the three models.

The global occurrence of these pressure oscillations inside the cavity was investigated by plotting the amplitude spectra of the pressure signals obtained at sidewall ports 1, 2 and 3 for the cavity with $L/W = 2$ as shown in Fig. 8. In addition to the existence of the dominant mode of oscillation corresponding to $St = 0{\cdot}259$, another prominent mode at frequency 15,230Hz is observed on the sidewalls of amplitude 170·5dB. This mode corresponds to a rather high St of 1·554. Such high St is usually observed for low amplitude oscillation generated in similar cases due to interaction of the large scale structures in the shear layer with the trailing edge. For the present case, resonant effects within the cavity seem to generate this high frequency, high amplitude oscillation at sidewall port 1 of the $L/W = 2$ model. Effect of this wave is observed at port 2 and 3 for the $L/W = 2$ cavity but with reduced amplitude. Reduction in the amplitude of dominant wave and the broadband fluctuations are also observed as one moves along the sidewall from the trailing edge to the leading edge of the cavity.

Amplitude spectra of pressure oscillations at the sidewall port 1 of all the three cavities are shown in Fig. 9. Discrete amplitude tones were present only for the cavity with $L/W = 2$. The acoustic signatures at the sidewall for the other two cavities were characterised by the existence of only low amplitude broadband noise. Exchange of fluid between the cavity and the freestream takes place due to flapping motion of the shear layer. As the shear layer comes out of the cavity, fluid from within the cavity is ejected into the freestream at the trailing edge[17]. For a partially spanning cavity, this exchange not only takes place at the trailing edge, but is also expected to occur along the cavity sidewalls. This exchange of mass along the sidewalls acts a mechanism of generation of oscillation along the sidewalls. High amplitude discrete peak for the $L/W = 2$ cavity implies more interaction with the freestream in this region for this model.

Variation of the non-dimensionalised cross correlation coefficient, η with the time lag (t) of the FFT of the pressure data is also plotted. Simultaneously sampled pressure signals from the leading and trailing edge ports are considered for the calculation of the cross correlation coefficient. The cross correlation coefficient and spectrogram of the pressure signal obtained at the leading and trailing edges of all the cavities are shown respectively in Figs 10 and 11. The dominant frequencies are observed to be existing all along the time the pressure data is sampled.

https://doi.org/10.1017/S0001924000007934 Published online by Cambridge University Press

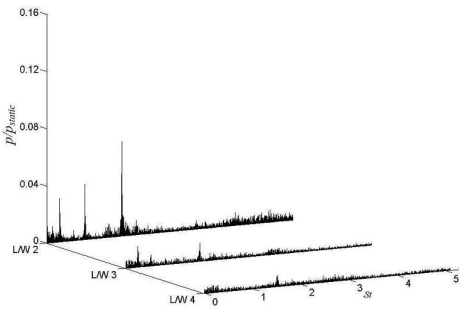


Figure 9. Amplitude spectra of pressure oscillation (sidewall port1) of partially spanning cavities.

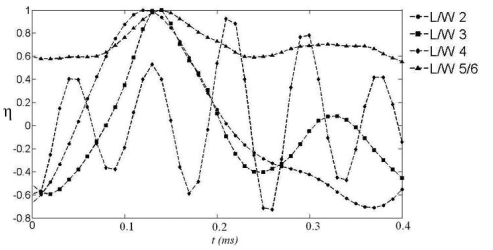


Figure 10. Cross correlation coefficient of leading and trailing edge port pressure signals.

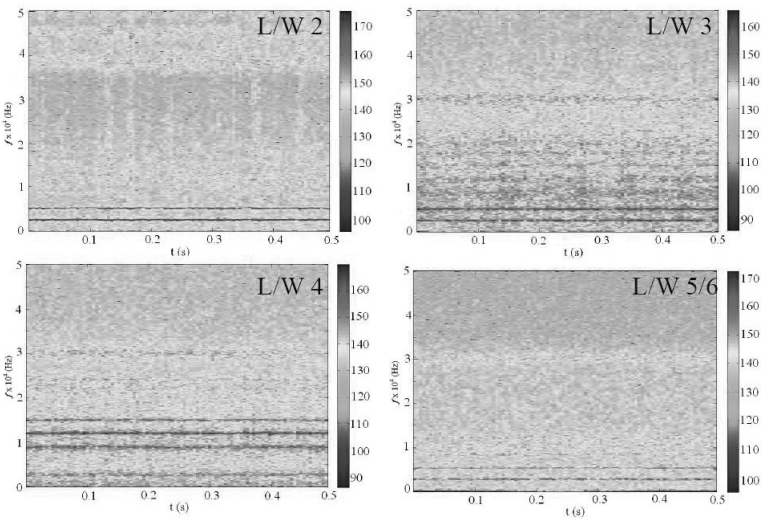


Figure 11. Spectrogram of trailing edge port pressure signals.

The maximum positive peak occurs at a time lag of approximately 0·14 ms for the wider models $L/W = 2$, $L/W = 3$ and the $L/W = 5/6$ cavity as is observed from the cross correlation plot shown in Fig. 10. Considering the cavity length of 50mm, the velocity of the disturbance is calculated to be about 350ms^{-1} which is approximately the velocity of an acoustic wave propagating inside the cavity. Maximum positive peak for the narrowest cavity is observed to be at a time lag of 0·22ms although there are multiple peaks observed at different time lags. Acoustic energy is observed to get distributed over multiple modes as the cavity narrows down. Spectrogram of the pressure signal was plotted to check the distribution of acoustic energy and the intermittency of existence of the different modes of oscillations. From the spectrogram plots shown in Fig. 11 most of the energy is observed to be concentrated with the dominant mode for the cavity with $L/W = 2$ whereas the energy is distributed over various modes for the other two partially spanning cavities. The colour bar on the right of each of the spectrogram plots gives the SPL in dB. Distribution of acoustic energy is observed to be organised and concentrated in lower modes with increase in cavity width.

https://doi.org/10.1017/S0001924000007934 Published online by Cambridge University Press

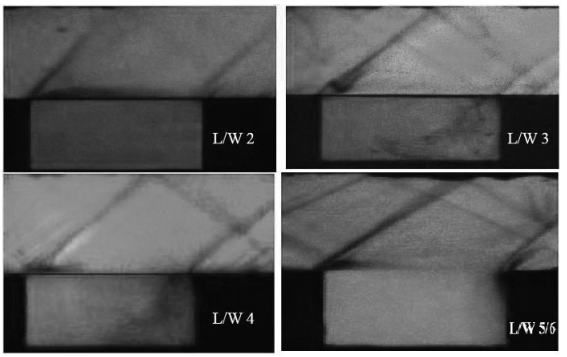


Figure 12. Time averaged Schlieren images.

3.2 Flow visualisation

Qualitative study of the wave structure and shear layer in the vicinity of the cavity was done through time averaged colour Schlieren technique for all the models. Images obtained during schlieren visualisation are shown in Fig. 12. Steep density gradients are observed at the leading and trailing edges of all the cavities. Unsteady movement of the shear layer in the vertical direction at the leading edge creates obstruction to the freestream supersonic flow and hence oblique shocks are found to form at the leading edge of the cavity. The flapping of the shear layer at the trailing edge causes the exposure of the edge to supersonic freestream flow thus generating another oblique shock at the trailing edge.

Difference in the shear layer thickness at the leading edge is apparent from the images obtained for models of $L/W = 2$ and $L/W = 4$. For the $L/W = 2$ model, the shear layer is observed to grow in thickness rapidly near the cavity lip just after the leading edge shock. Thickness of the shear layer for the $L/W = 4$ cavity is less as compared to the cavity of $L/W = 2$. The nature of acoustic disturbance near the leading edge may have a direct impact on the thickness of the shear layer. Acoustic disturbance has been observed to be of much higher amplitude for the cavity of $L/W = 2$.

The thickness of the shear layer at the leading edge in turn affects the shock angle at the leading edge. The shock angle is observed to be higher for the $L/W = 2$ cavity than the other models. The trailing edge shock angle is observed to be same in all the cases implying that the trailing edge is exposed to identical freestream conditions for all the cavities.

A region of high density gradient is observed at the bottom corner of trailing edge wall for the narrower cavities. This could be due to the movement of the vortical structures along the trailing edge and along the floor following the circulation present at the trailing edge. Similar observation was made also by Zhang[21].

Instantaneous flow visualisation is performed to study the unsteady nature of flow past cavities. Wave structure of supersonic flow past cavities has been explained by many previous researchers. The illustration of the wave structure shown in Fig. 13 is by Heller and Delfs[9]. In Fig. 13, wave 1 depicts the upstream moving acoustic wave inside the cavity and it's projection in the mainstream. When the externally trailed front reaches the leading edge it detaches from the cavity internal stem and swims off into the external medium. A quasi-steady compression shock appears each time the shear layer is deflected upwards at the leading edge. This wave is shown in Fig. 13 as wave 2. Each time the shear layer dives into the cavity the trailing edge is exposed to the supersonic freestream. This results in appearance of a bow shock shown as wave 3 in Fig.13. During the upward motion of the shear layer at the trailing edge and its subsequent

https://doi.org/10.1017/S0001924000007934 Published online by Cambridge University Press

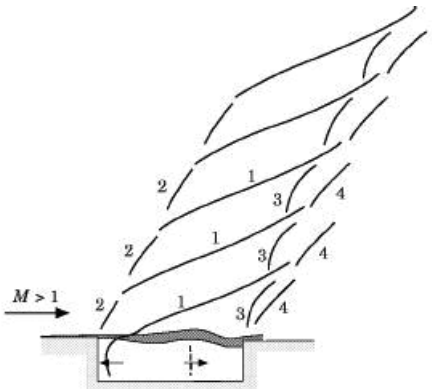


Figure 13. Wave structure for supersonic flow past cavities[9].

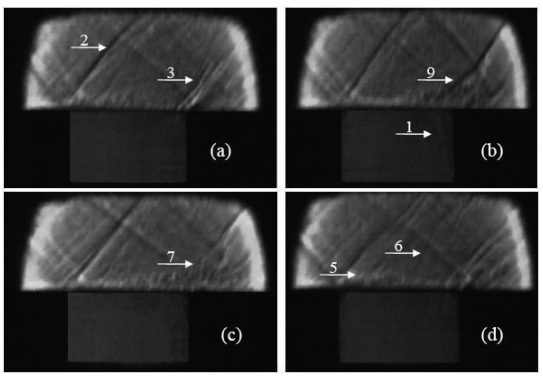


Figure 14. Instantaneous shadowgraph images of flow over cavity with $L/W = 2$.

reattachment at the surface just beyond the trailing edge a compression wave shown as wave 4 occurs.

Cavities that excite discrete oscillations exhibit distinct features like leading and trailing edge shock, waves traveling inside the cavities and their projection in the mainstream flow, vortex roll up and shock waves associated with unsteady shear layer. Periodic nature of these unsteady oscillations enables presentation of the associated flow features as sequential images obtained during instantaneous shadowgraph visualisation.

Different waves and flow structure occurring in the vicinity of the cavity with $L/W = 2$ is shown in Fig. 14(a)–(d). Apart from the features already discussed with reference to Fig. 13, some additional observations were made which are described subsequently in the paper. Images were acquired at a rate of 1,500fps. Strong shock in the mainstream is observed at the leading edge of the cavity due to deflection of shear layer as marked by wave 2. As the shear layer starts diving into the cavity at the trailing edge, a bow shock appears seen as wave 3 in Fig 14(a), and the shear layer is observed to impinge on the trailing edge. A compression wave (1) is produced due to the impingement which travels in the upstream direction inside the cavity. Projection of this wave is noticed in the mainstream near the trailing edge in Fig. 14(b). This wave immediately disturbs the shear layer in the vicinity of the trailing edge which results in vortex roll up and shear layer coming out near the trailing edge. Multiple waves emanating from the cavity near the trailing edge coalesce to form a lambda shock structure marked as 9 in Fig. 14(b).

https://doi.org/10.1017/S0001924000007934 Published online by Cambridge University Press

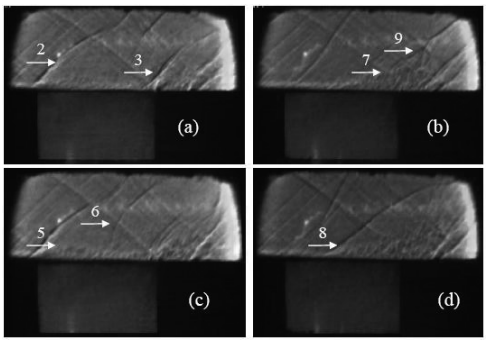


Figure 15. Instantaneous shadowgraph images of flow over cavity with L/W= 3.

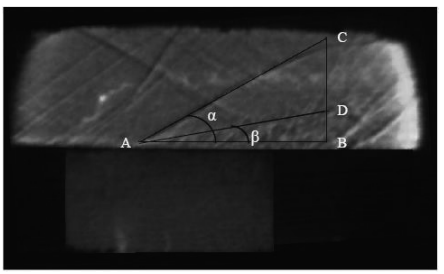


Figure 16. Instantaneous shadowgraph image of flow over cavity with L/W = 3 showing wave 8.

As the shear layer comes out near the trailing edge, exchange of fluid between cavity and mainstream takes place and considerable amount of disturbances is generated in the mainstream marked as structure 7. These disturbances in turn create obstruction to the mainstream supersonic flow and generate bow shocks as seen in Fig. 14(d) and marked as 6. As the wave 1 travels inside the cavity it disturbs the shear layer and causes the shear layer to roll up into the mainstream before the leading edge shock is generated.

Similar features were observed for the cavity with $L/W = 3$. Images obtained for this model is shown in Fig. 15(a)-(d). The lambda shock structure near the trailing edge of the cavity marked as 9 and the bow shock (6) at half cavity length due to the obstruction caused by upward movement of shear layer are clearly seen in Fig. 15(b) and (c). In addition to these features, another prominent wave marked as 8 was observed during the experiments. Shear layer coming out of the cavity due to upward deflection by the moving acoustic wave inside the cavity seemed to be the reason behind generation of this wave.

The wave angle and the shear layer deflection angle with reference to the mainstream flow direction were calculated from the pixel values of the points A, B, C and D for this instantaneous image as shown in Fig. 16. The maximum shear layer deflection angle β was obtained as 9·492° and the wave angle α as 28·94°. Flow Mach number in the vicinity of station A in the mainstream was approximately 1·6234 from the numerical calculations described later. For M = 1·6234, and a deflection angle of 9·492°, the actual wave angle was established to be much higher than 28·94°. This wave angle of 28·94° was also observed to be higher than the Mach wave angle for flow at M = 1·6234, but for a very less deflection angle $\beta < 2°$. It is thus concluded that the effective β that the mainstream flow experiences is less than that of the shear layer deflection angle.

Flow phenomena associated with the narrowest cavity with L/W ratio 4 is similar to the other two cavities though the disturbances created in the main flow and the shear layer structure is different from them. This is evident from the images obtained from shadowgraph visualisation for this cavity which has been shown in Fig. 17(a)-(c). As the shear layer comes out of the cavity near the trailing edge, large scale structures are observed in the freestream for the wider cavities as seen in Figs 14(c) and 15(b). The structures are not as prominent and large for the narrowest cavity marked as 7 in Fig. 17 which also shows an imprint of the trailing edge bow shock. This is indicative of the shear layer fluctuating at a different rate than the other two cavities.

Vortex roll up and wave generated due to deflection of shear layer is observed for the narrowest cavity and is marked as 5 and 8 respectively in Fig. 17. Overall, the flow in the mainstream in the vicinity of the narrowest cavity was observed to be much subdued as compared to the wider

https://doi.org/10.1017/S0001924000007934 Published online by Cambridge University Press

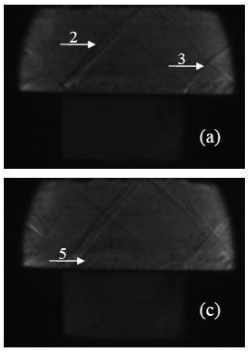


Figure 17. Instantaneous shadowgraph images of flow over cavity with $L/W = 4$.

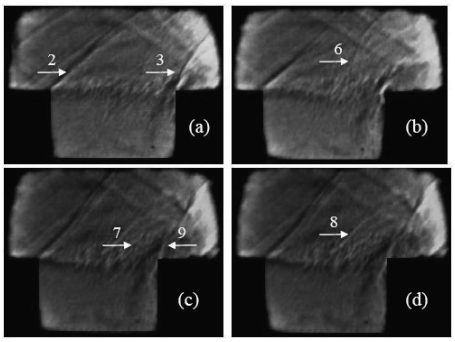


Figure 18. Instantaneous shadowgraph images of flow over $L/W = 5/6$ cavity.

cavities. The roll up vortices forming the shear layer is seen to be confined to a narrow region along the cavity lip of all the three models which moves along the trailing edge wall to the bottom of the cavity. Overall, not much activity is visible inside the cavity except at the trailing edge for the cavities with $L/W = 2$ and $L/W = 3$.

Instantaneous shadowgraph images for the baseline cavity model are shown in Fig. 18. Deflection of the shear layer into the cavity and subsequent exposure of the trailing edge to the supersonic mainstream flow generates a bow shock at the trailing edge of the cavity marked as 3 in Fig. 18. Similar features like other models are also observed for this case and the different flow and wave structures are marked accordingly as shown in Fig. 18(a)-(d). Vigorous interaction of the shear layer with the trailing edge was observed as in the case of the wider partially spanning cavities and is indicated as 7.

3.3 Numerical analysis

Numerical studies of supersonic confined flows are done for all the models using unsteady, 3D, explicit calculations by commercially available finite volume code Fluent. Unsteady Reynolds averaged Navier Stokes (RANS) is used as the preferred numerical technique due to unsteady nature of the flow marked by periodic vortex shedding and self sustaining pressure oscillations[22]. Explicit scheme has been used for time marching and the results obtained has been displayed as computed flow structure after the flow parameters converged to the desired boundary conditions. As the time scales governing the flow over cavities is quite small, explicit scheme was used as solution accuracy predominated over linear stability for the present case. As the global time step used for the calculation was small, convergence to steady state was achieved over a long period of time for each of the cases. Geometrical configurations of all the models are generated using Gambit, commercially available modeling software. The computational domain is also meshed into structured hexahedral cells using Gambit. The number of cells varied from 687,600 for the narrowest cavity to 918,000 for the 2D cavity model. Computational grid for the widest 3D cavity is shown in Fig. 19. Outline of the entire 3D computational domain is shown in Fig. 20.

Standard k-ε model is used to estimate turbulence. Inlet stagnation pressure of 5bar and a test section M_∞ of 1·7 are used in the numerical solution. Pressure inlet and pressure outlet were used as boundary conditions and air under ideal gas conditions as the working fluid. Iterations were done till the solution converged to a residual value of 10e–06. Grid independence study was done and the grid was refined till the area weighted average wall y^+ value 10mm upstream of the cavity

https://doi.org/10.1017/S0001924000007934 Published online by Cambridge University Press



Figure 19. Computational grid along the axial plane of the test section.

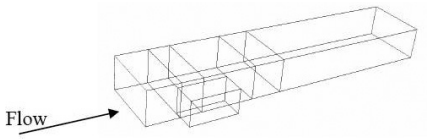


Figure 20. Computational domain.

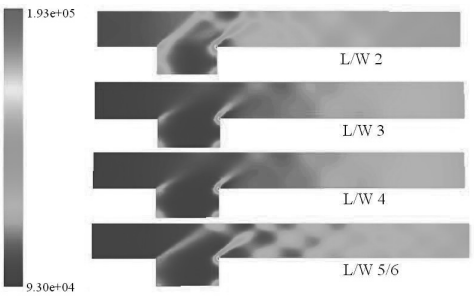


Figure 21. Comparison of static pressure (in Pa) distribution along the midplane of test section.

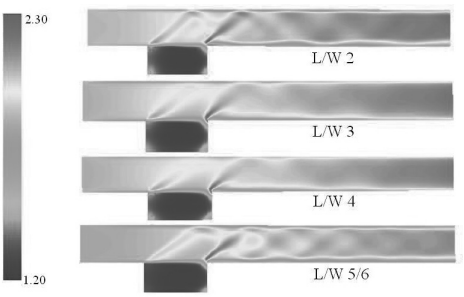


Figure 22. Comparison of density (in kg/m^3) variation along the midplane of test section.

leading edge for all the models came down to below 19. All numerical results presented here are taken from these converged solutions.

Static pressure and density variations are plotted along the axisymmetric mid plane of the test section to study the flow structure. A comparative result of pressure variation of all the test cases is shown in Fig. 21. It is evident from Fig. 21 that the locations of static pressure variations in all the cases remain same. There is considerable change in pressure in the vicinity of the leading and trailing edges of the cavity. This can be attributed to presence of shocks at these locations due to the flapping of the shear layer. The shear layer over the open cavity top is visible in Fig. 22 which shows the variation of density along the midplane of the test sections. A steep density gradient is observed at the leading and trailing edge of the cavity signifying the presence of shocks at these locations.

Although the shock structure in all the four cases appear to be almost identical, the leading edge shock angle for the widest partially spanning cavity is observed to be more than the other cavities indicating that leading edge shock is stronger for the $L/W = 2$ cavity. This underlines the fact that the shear layer thickness is more at the leading edge for the widest cavity as was observed during flow visualisation.

Protrusion of the shear layer into the freestream at the trailing edge is noted from the density contours shown in Fig. 22. The density gradient appears to spread out into the mainstream for the $L/W = 2$ cavity as opposed to the other models, indicating a more pronounced effect of this cavity on the mainstream flow. Fluid density in the region above the $L/W = 2$ cavity between the leading and trailing edge shock is observed to be higher. The velocity vector plots along the axisymmetric midplane of the test section of the models shows existence of one single vortex for all the cases as shown in Fig. 23. The vectors are colored according to velocity and the color bar on the left of Fig. 23 indicates the velocity range in m/s. It is observed that the freestream velocity is within 4·5% of the measured experimental value. This mismatch with the experimental value may be due to the approximations made while defining the turbulence model for the numerical simulations. No

https://doi.org/10.1017/S0001924000007934 Published online by Cambridge University Press

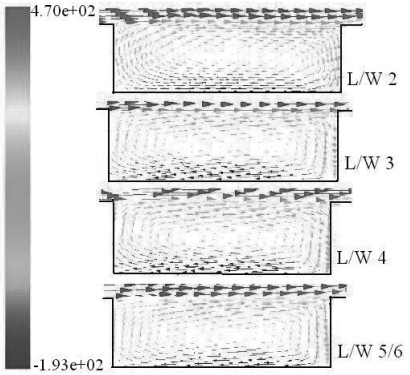


Figure 23. Existence of single vortex along the test section midplane.

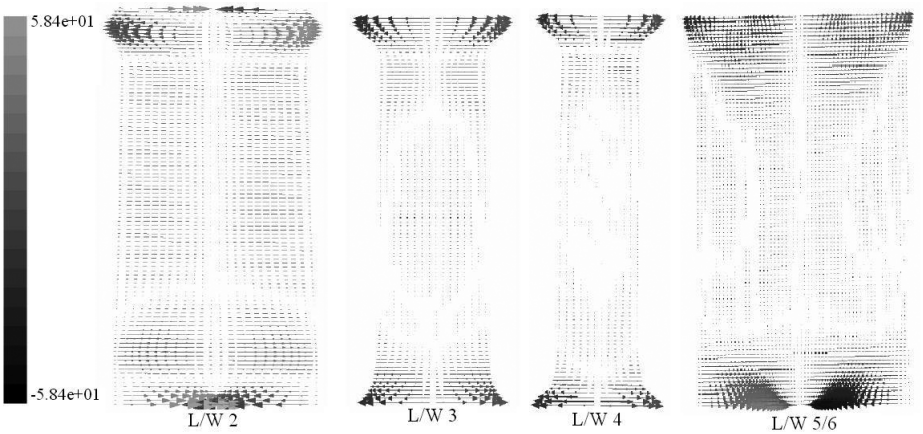


Figure 24. Lateral velocity along cavity midplane.

secondary vortices are observed along the axial midplane of the cavity as seen in Fig. 23.

Velocity vectors along the horizontal midplane of the cavity are shown in Fig. 24 where the gray scale colour bar on the left indicates the velocity range in ms^{-1}. Lateral movement of flow is observed along this plane for the $L/W = 2$ cavity. Fig. 25 shows the lateral movement of flow in the vicinity of the leading edge of this cavity in the horizontal midplane. The outward flow observed 15mm downstream of the cavity leading edge for this model was not observed for the other cavities. For cavities with $L/W = 3$ and 4, the lateral movement is limited to only in the vicinity of the leading and trailing edge. Velocity vectors present in lateral directions signifies existence of vortical flow. Two lateral vortices were observed to be present inside the cavity of $L/W = 2$ whereas only one weak vortex is seen to be present for the other two cavities.

To gain an insight into the varying amplitude of pressure oscillations observed during experiments, the rate of fluid exchange between the mainstream and the cavity was computed numerically for the incoming flow of $M_\infty = 1{\cdot}7$ for all the cases. The mass flow rate m_c through the open cavity top is calculated as follows:

$$m_c = \int \rho \vec{v}.d\vec{A} = \sum_{i=1}^{n} \rho_i \vec{v}_i.\vec{A}_i \qquad \ldots (2)$$

https://doi.org/10.1017/S0001924000007934 Published online by Cambridge University Press

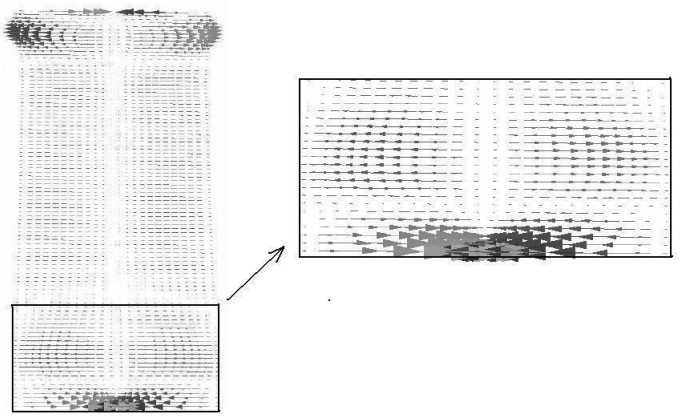


Figure 25. Lateral velocity in the vicinity of the leading edge of $L/W = 2$ cavity.

Table 2
Comparison of mass exchange between cavity and mainflow for all cases

Model	m_c (kg/s)	V_c (m^3)	ε
$L/W = 2$	$47{\cdot}687 \times 10^{-5}$	$3{\cdot}125 \times 10^{-5}$	15·26
$L/W = 3$	$6{\cdot}598 \times 10^{-5}$	$2{\cdot}083 \times 10^{-5}$	3·167
$L/W = 4$	$0{\cdot}652 \times 10^{-5}$	$1{\cdot}562 \times 10^{-5}$	0·417
$L/W = 5/6$	$69{\cdot}71 \times 10^{-5}$	$7{\cdot}5 \times 10^{-5}$	9·295

The mass flow rate is computed by dividing the open cavity top into n number of facets and summing the mass flow rate through them after the solution converged to a steady state. The computed mass flow rate m_c through the open cavity top surface for all the cases is given in Table 2.

Rate of mass exchange between the widest cavity and the mainstream is calculated to be highest as seen in Table 2. Ratio of mass flow rate to volume of the cavity was observed to be much higher for the partially spanning cavity model with $L/W = 2$. The amplitude of pressure oscillations was observed to be much higher for this model as compared to the other three models. It is observed that the amplitude of pressure oscillations increases with increase in ε.

4.0 CONCLUSIONS

3D cavity induced acoustic oscillations for different cavity widths have been investigated at freestream supersonic flow of $M_\infty = 1{\cdot}7$. Effects of both partially spanning and full span cavity on the flow characteristics have been studied. Mode frequencies of discrete pressure oscillation that are seen to exist in the flow field are observed to be independent of cavity width. A jump in dominant frequency of pressure oscillation is observed as the cavity narrows down from L/W ratio of 3 to 4. Multiple dominant peaks are also observed for the narrowest cavity. It appears that the jump in the frequency of the dominant mode of oscillation observed in the present study is due to fluid resonant effects. The high amplitude of pressure oscillation observed for the widest partially spanning cavity is due to larger mass addition near the trailing edge caused by the flapping shear layer. Suppression of vibrations along the sidewalls of the narrowest cavity is evident from the results of unsteady pressure measurement. Time averaged flow visualisation shows the details of

https://doi.org/10.1017/S0001924000007934 Published online by Cambridge University Press

shock structure formed due to the presence of unstable shear layer along the length of the cavity. Insight into the mechanism of quasi steady shock formation, propagation of acoustic wave inside cavity and the unsteady shear layer structure is provided by instantaneous flow visualisation. Disturbances induced in the mainstream by the $L/W = 2$ cavity are observed to be much higher than the other models. For the case of the narrowest cavity model, the mainstream flow is observed to be quiescent than the wider cavities. The above facts indicate that the disturbance caused in the main flow is directly affected by mass interaction between the cavity and the mainstream. Amplitude of pressure oscillations, disturbances created in the mainstream and interaction between the mainstream flow and the confined fluid flow in the cavity are observed to be more dependent on the cavity mass flow rate to volume ratio than the mass flow rate only. This ratio, ε was found to have intense effect on the amplitude of pressure oscillations generated by the cavities. Similar trends are obtained in the results of numerical analysis. Lateral velocities inside the cavity are more pronounced along the whole of cavity length for the $L/W = 2$ cavity whereas it is limited to the leading and trailing edge of the narrower cavity. This indicates the presence of a strong lateral vortical structure for the widest cavity and the dependency of the three dimensionality of the flow on the cavity width.

REFERENCES

1. KRISHNAMURTHY, K. Acoustic radiation from two-dimensional rectangular cutouts in aerodynamic surface, 1955, NASA-TN-3487.
2. ROSSITER, J.E. Wind tunnel experiments on the flow over rectangular cavities at subsonic and transonic speeds, reports and memoranda No 3438, 1964, Aeronautical Research Council, pp 1-36.
3. HELLER, H.H, HOLMES, D.G and COVERT, E.E. Flow induced pressure oscillations in shallow cavities, *J Sound and Vibration*, 1971, **18**, (4), pp 545-553.
4. BILANIN, A.J. and COVERT, E.E. Estimation of possible excitation frequencies for shallow rectangular cavities, *AIAA J*, 1973, **11**, (3).
5. YU, K.H. and SCHADOW, K.C. Cavity Actuated supersonic mixing and combustion control, *J Combustion and Flame*, 1994, **99**, pp 295-301.
6. YAKAR, A.B. and HANSON, R.K. Cavity flame holders for ignition and and flame stabilization in scramjets: an overview, *J Propulsion and Power*, 1998, **17**, (4), pp 869-877.
7. ROCKWELL, D. and NAUDASCHER, E. Review — self sustaining oscillations of flow past cavities, *J Fluids Eng*, June 1978, **100**, (6), pp 152-165.
8. TAM, C.K.W. and BLOCK, P.J.W. On the tones and pressure oscillations induced by flow over rectangular cavities, 1978, *J Fluids Eng*, **89**, Part 2.
9. HELLER, H. and DELFS, J. Cavity Pressure oscillations: the generating mechanism visualized. *J Sound and Vibration*, 1996, **196**, (2), pp 248-252.
10. BLOCK, P.J.W. Noise response of cavities of varying dimensions at subsonic speeds, 1976, NASA TN D 8351.
11. MAULL, D.J. and EAST, L.F. Three dimensional flow in cavities, *J Fluid Mech*, 1963, **16**, pp 620-632.
12. SHEIH, C.M. and MORRIS, P.J. Comparison of two and three dimensional turbulent cavity flows, January 2001, AIAA 2001-0511.
13. SOEMARWOTO, B.I. and KOK, J.C. Computations of three-dimensional unsteadysupersonic cavity flow to study the effect of downstream geometries, November 2001, NLR-TP-2001-446.
14. ZHUANG, N., ALVI, F.S., ALKISLAR, M.B. and SHEIH. C. Supersonic cavity flows ad their controls, *AIAA J*, 2006, **44**, ()9, pp 2118-2156.
15. CHOI, H., MUN, P. and KIM, J. Numerical analysis of subsonic flow around a three dimensional cavity, *J Mech. Science and Tech*, 2009, **23**, pp 1702-1709.
16. WOO, C., KIM, J. and LEE, K. Three dimensional effects of supersonic cavity flow due to the variation of cavity aspect and width ratios, *J Mech. Science and Tech*, 2008, **22**, pp 590-598.
17. GRUBER, M.R, BRAULE, R.A., MATHUR, T. and HSU, K.Y. Fundamental studies of cavity based fameholder concepts for supersonic combustors, July 1999, AIAA Paper 99-2248.

https://doi.org/10.1017/S0001924000007934 Published online by Cambridge University Press

18. ZHANG, X. and EDWARD, J.A. An investigation of supersonic oscillatory cavity flows driven by thick shear layers, *Aeronaut J*, 1990, pp 355-364.
19. ROWLEY, C.W., COLONIUS, T. and BASU, A.J. On self sustained oscillations in two-dimensional compressible flow over rectangular cavities, *J Fluid Mech*, 2002, **455**, pp 315-346.
20. HANDA, T. and MASUDA, M. On the jump in the frequency of acoustic oscillations in supersonic flows over rectangular cavity, *Physics of Fluids*, February, 2009, **21**, 026102, pp 1-7.
21 ZHANG, X. Compressible cavity flow oscillation due to shear layer instabilities and pressure feedback, *AIAA Journal*, 1995, **33**, (8), pp 1404–1411.
22. SHARMA, M., RISHIKESH, V., SHET, U.S.P. and SUNDARARAJAN, T. Enhancement of fuel air mixing in supersonic flow by wall mounted opposed cavity, Proceedings of ISABE-2005-1112, pp 1-9.

https://doi.org/10.1017/S0001924000007934 Published online by Cambridge University Press